Electronic Supplementary Information (ESI)

Highly stable Ru-complex-based metal-covalent organic frameworks as novel type of electrochemiluminescence emitters for ultrasensitive biosensing

Yang Yang,[a] Haicheng Jiang,[b] Jialu Li,[b] Jialing Zhang,[a] Shu-Zhen Gao,[a] Mei-Ling Lu,[a] Xin-Yue Zhang,[a] Wenbin Liang,[a] Xiaoqin Zou,*[,b] Ruo Yuan*[,a] and Dong-Rong Xiao*[,a]

[a]*Key Laboratory of Luminescence Analysis and Molecular Sensing (Southwest University), Ministry of Education, College of Chemistry and Chemical Engineering, Southwest University, Chongqing 400715, P. R. China*

[b]*Faculty of Chemistry, Northeast Normal University, Changchun 130024, P. R. China*

*Corresponding author. Tel: +86-23-68252360; fax: +86-23-68254000.

E-mail address: xiaodr98@swu.edu.cn (D. R. Xiao); yuanruo@swu.edu.cn (R. Yuan); zouxq100@nenu.edu.cn (X. Zou).

Table of Contents

S-1 Experimental section

S-1.1 Materials and reagents

Tris(4,4′-dicarboxylicacid-2,2′-bipyridyl)ruthenium(II) dichloride ($[Ru(dcbpy)_3]Cl_2$) was bought from Suna Tech Inc. (Suzhou, China). 1,2,4,5-benzenetetramine tetrahydrochloride (BTA·4HCl) and polyphosphoric acid (PPA) were purchased from Adamas (Shanghai, China). Tripropylamine (TPrA) was bought from Shanghai Macklin Biochemical Co. Ltd. (Shanghai, China). Gold chloride ($HAuCl_4$) and hexanethiol (HT) were bought from Sigma-Aldrich Co. (St. Louis, MO, USA). Exonuclease III (Exo III) was bought from Thermo Fisher Scientific Inc. (Shanghai, China). Nb.BbvCI was purchased from TaKaRa Biotechnology Co., Ltd. (Dalian, China). All the oligonucleotides (Table S1) utilized in this work were synthesized by Sangon Biotech. Co. Ltd. (Shanghai, China). Before use, the H1 and H2-Fc were denatured at 95 ^oC for 5 min and slowly chilled to room temperature to form the hairpin structure. The buffers involved in this work were shown as follows. DNA store buffer (pH 7.4): 1 × TE buffer (10 mM Tris-HCl and 1.0 mM ethylenediaminetetraacetic acid (EDTA)). Annealing buffer (pH 8.0): 10 mM Tris-HCl, 1.0 mM EDTA, and 150 mM NaCl. Aging buffer (pH 7.4): 10 mM phosphate buffer solution (PBS, 1.9 mM NaH_2PO_4, 8.1 mM K_2HPO_4,), 0.2 M NaCl, and 1.0 mM EDTA. The detection phosphate-buffered solution (PBS, pH 7.0): 0.1 M K_2HPO_4, 0.1 M NaH_2PO_4, and 0.1 M KCl. Ferricyanide/ferrocyanide mixed solution ($[Fe(CN)_6]^{3-/4-}$, pH 7.0, 5.0 mM) was prepared by dissolving potassium ferricyanide and potassium ferrocyanide with 0.1 M PBS. All chemicals were analytical grade and used without further purification. All solutions were prepared using deionized water (18.2 $M\Omega \cdot cm^{-1}$) obtained from a Milli-Q water purification system (Millipore, USA).

Table S1 The oligonucleotide sequences used in this work

Name	Sequences (5' to 3')
H1	NH_2-TTTTTTTTTTTTAATCGCCTCAGCTGATACATTGTTTGCTATTTTAGCAAACAATGTATCACGATTAGCATTAA
miRNA-155	UUAAUGCUAAUCGUGAUAGGGGU
H2-Fc	NH_2-TTTTTTCATGCAATGTATCAGCTGAGGCGATTACATTGCATG-Fc
S1	NH_2-TTTTTTTTTTTTAATCGCCTCAGCTGATACATTGTTTGCTATTT
miRNA-21	UAGCUUAUCAGACUGAUGUUGA
miRNA-122	UGGAGUGUGACAAUGGUGUUUG
miRNA-141	UAACACUGUCUGGUAAAGAUGG
miRNA-199a	ACAGUAGUCUGCACAUUGGUUA
miRNA-203a	AGUGGUUCUUAACAGUUCAACAGUU
miRNA-429	UAAUACUGUCUGGUAAAACCGU
TBA	GGTTGGTGTGGTTGG

S-1.2 Apparatus and measurements

The electrochemical measurement was carried out with a CHI760E electrochemical workstation (Shanghai Chen Hua Instrument, Shanghai, China) from -0.2 V to 0.6 V. The ECL measurement was performed on a model MPI-A electrocheminescence analyzer (Xi'an Remax Electronic Science & Technology Co. Ltd., Xi'an, China) from -1.3 V to 1.25 V in 2 mL of PBS (pH 7.0) solution containing 25 mM TPrA. The scanning rate was 0.3 V/s and the voltage of the photomultiplier tube was set at 800 V. ECL, cyclic voltammetry (CV), and electrochemical impedance spectroscopy (EIS) measurements equipped with a conventional three-electrode system including a glassy carbon electrode (GCE, Φ = 4 mm) working electrode, a platinum wire counter electrode, and an Ag/AgCl (saturated KCl) reference electrode. Before use, the GCE was seriously polished with 0.3 and 0.05 μm alumina powders and then cleared thoroughly with deionized water to acquire a mirror-like surface. After each

modification, the electrode was rinsed with deionized water. Powder X-ray diffraction (PXRD) patterns were collected on an XD-3 X-ray diffractometer with Cu Kα radiation (Purkinje, China). The surface morphology was characterized by transmission electron microscopy (TEM, JEOL Ltd, Tokyo, Japan). Scanning electron microscopy (SEM) and energy-dispersive X-ray spectroscopy (EDS) mapping images were taken using Gemini 300 microscope. Nitrogen adsorption-desorption measurement was performed on QUADRASORB SI020503 adsorption apparatus at 77.3 K. Before the measurement, the sample was outgassed under vacuum at 125 ^{o}C for 24 hours. The Fourier transform infrared (FT-IR) spectra were carried out using Spectrum GX FTIR spectroscopy system (PerkinElmer, USA). UV-vis absorption spectra were carried out on a UV-2450 UV-vis spectrophotometer (Shimadzu, Tokyo, Japan). Photoluminescence (PL) spectra were carried out on an F-7000 spectrofluorophotometer (Hitachi, Tokyo, Japan).

S-1.3 Synthesis of gold nanoparticles (AuNPs)

AuNPs were synthesized according to previous reports with some modifications.[S1,S2] Briefly, 2.5 mL sodium citrate (1%, w/v) was added into 100 mL boiled $HAuCl_4$ (0.01%, w/v) solution under violent stirring. The mixture was continued boiling for 10 min under stirring when the color turned from yellow to red violet. Then, the mixture solution was cooled to room temperature, and AuNPs were thus synthesized. The prepared AuNPs solution was stored in brown glass bottles at 4 ^{o}C for further use. The UV-vis absorption spectrum of AuNPs was shown in Fig. S1, which was consistent with that reported in the literature.[S3] This result demonstrated that the AuNPs were successfully synthesized.

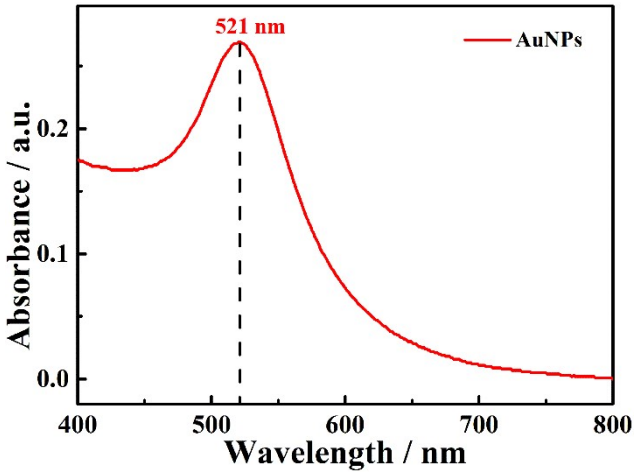

Fig. S1 UV-vis absorption spectrum of AuNPs.

S-1.4 Synthesis of the Ru-MCOF

$[Ru(dcbpy)_3]Cl_2$ (27 mg, 30 μmol), BTA·4HCl (26 mg, 90 μmol), and PPA (3 mL) were placed in a Teflon-lined stainless-steel autoclave. The mixture was heated at 150 °C for 24 h and then heated at 180 °C for 24 h. After the pH of the resulting mixture was adjusted to 8-9 with saturated $NaHCO_3$ solution, black powder was precipitated. After centrifugation, the powder was collected and respectively washed with water, methanol, and acetone in a Soxhlet extractor for 12 h, and then dried at 100 °C under vacuum for 6 h to give the Ru-MCOF.

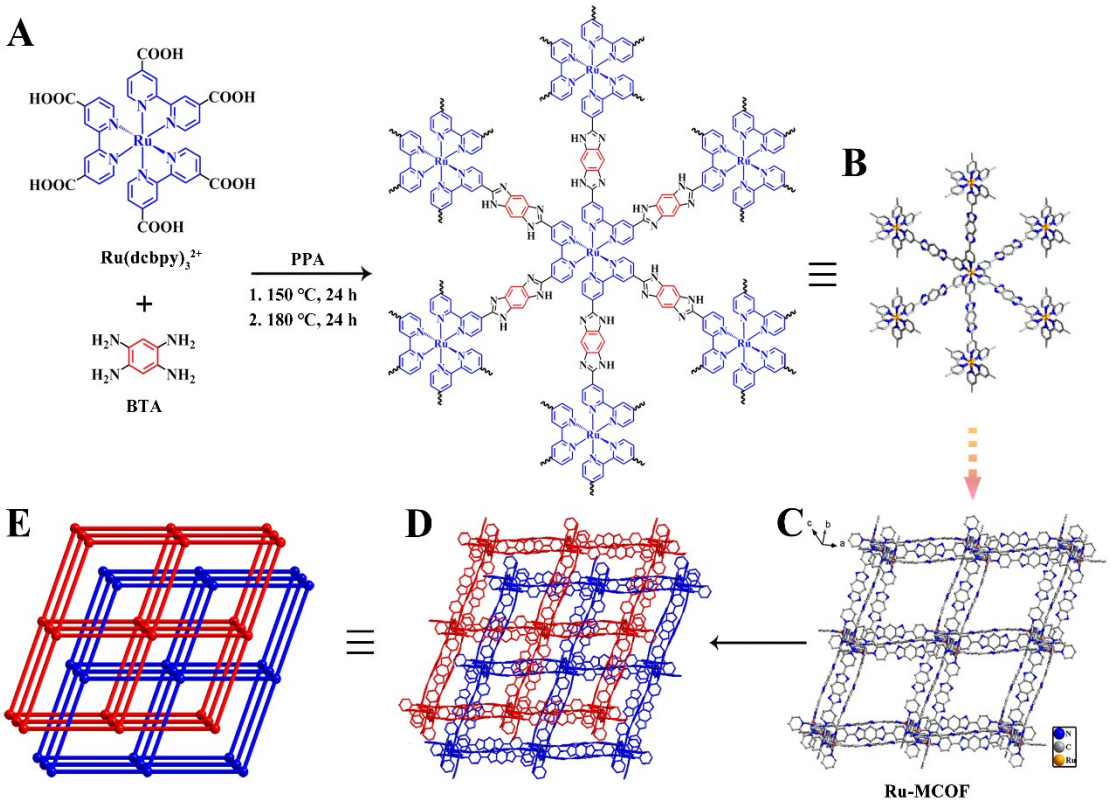

Scheme S1 (A, B) Synthesis of the Ru-MCOF. (C) The single 3D network of the Ru-MCOF. The elements are represented as N, blue ball; C, gray ball; Ru, orange ball. (D) The two-fold interpenetrating network of the Ru-MCOF with (E) pcu topology.

S-1.5 Cell culture and cell lysate preparation

The human breast cancer cells (MCF-7) and cervical cancer cells (Hela) were purchased from the cell bank of the Chinese Academy of Sciences (Shanghai, China). The MCF-7 and Hela cells were cultured in Dulbecco's modified Eagle's medium containing 10% fetal bovine serum, 100 U/mL penicillin, and 1% non-essential amino acids at 37 °C with a humidified atmosphere (95% air and 5% CO_2). Then, the total RNA extraction for the real sample detection was obtained using the Trizol Reagent Kit (Invitrogen Biotechnology Co., Ltd) according to the manufacturer's protocol. Firstly, the cell pellets were added to the appropriate Trizol Reagent and oscillated three times. Then, the processed cell pellets were transferred to an RNase-free centrifuge tube and incubated at room temperature for 5-10 min to ensure complete cell disruption.

Afterward, the processed RNA pellets were washed with 75% ethanol and re-dissolved in RNase-free water, and stored at -80 °C for further use.

S-1.6 Preparation of the H1@AuNPs

First, a mixture containing 120 μL of H1 (5 μM), 140 μL of PBS (10 mM), and 500 μL of AuNPs was stirred for 5 h at 35 °C. Then, 30 μL of aging buffer solution was added into the above reaction mixture every 30 min until the final concentration of NaCl reached 0.6 mM. The salting process was followed by overnight incubation at 35 °C. Afterward, the excessive H1 was removed by centrifugation twice at 14000 rpm for 15 min. The H1@AuNPs were finally resuspended in 1 mL of 10 mM PBS buffer and stored at 4 °C for further use.

S-1.7 Preparation of the S1@AuNPs

20 μL of H1@AuNPs and 5 μL of Exo III (2 U/μL) were mixed with 20 μL of miRNA-155 of various concentrations. The mixture was incubated at 35 °C with stirring for 50 min. Thereafter, the reaction process was terminated by incubation at 70 °C for 20 min to obtain the S1@AuNPs.

S-1.8 Fabrication of the ECL biosensor

First, 10 μL of Ru-MCOF (1 μM) was coated on the cleaned GCE surface. Then, 10 μL of AuNPs was modified on the Ru-MCOF/GCE. Subsequently, the AuNPs/Ru-MCOF/GCE was incubated with H2-Fc (2 μM, 20 μL) overnight. Afterward, HT (1 mM, 10 μL) was decorated on the surface of the obtained electrode for 50 min at room temperature. Finally, 10 μL of the S1@AuNPs and 2 U of Nb.BbvCI were incubated on the resultant electrode surface for 30 min at room temperature.

S-1.9 The measurement of ECL emission spectra for MCOF and $[Ru(dcbpy)_3]Cl_2$

The ECL emission spectra were measured on a Newton EMCCD spectroscopy detector (Andor Co., England) combined with an electrochemical workstation (Vertex, Ivium, Netherlands) based on a conventional three-electrode system (a bare or modified GCE (Φ = 4 mm) as the working electrode, Ag/AgCl (saturated KCl) as the reference electrode, and a Pt wire as counter electrode). Concretely, the Ru-MCOF/GCE and $[Ru(dcbpy)_3]Cl_2$/GCE were performed in 2 mL PBS (0.1 M, pH 7.0) solution containing 25 mM TPrA. The scanning potential was set as -1.3 - 1.25 V with a scanning rate of 0.3 V/s.

S-2 Results and discussion

S-2.1 Characterization of Ru-MCOF

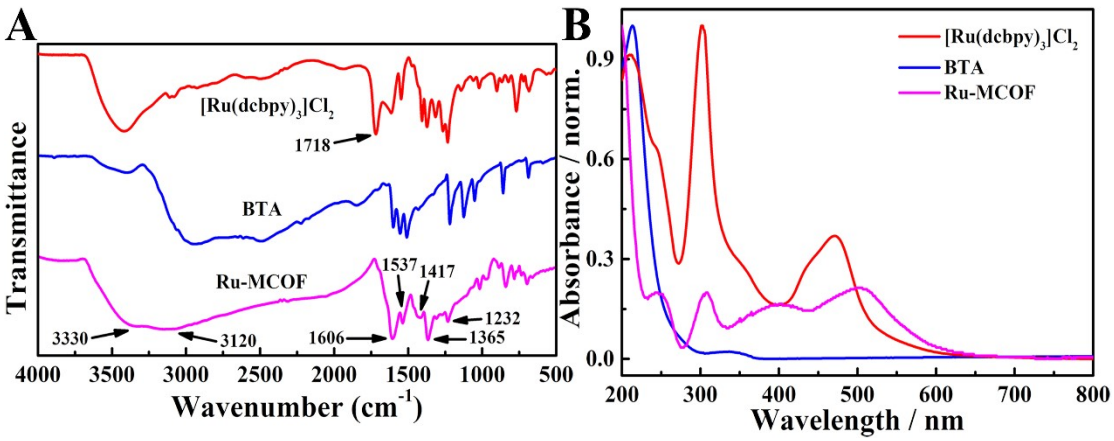

Fig. S2 (A) FT-IR and (B) UV-vis absorption spectra of the $[Ru(dcbpy)_3]Cl_2$, BTA, and Ru-MCOF.

Table S2 Fractional atomic coordinates for the unit cell of the Ru-MCOF

Ru-MCOF		Space group: $R3c$ (no. 161) $a = b = 30.2178$ Å, $c = 43.7592$ Å $\alpha = \beta = 90^o$, $\gamma = 120^o$ $R_{wp} = 1.50\%$, $R_p = 1.18\%$		
N1	N	0.26501	0.62945	0.94171
C2	C	0.78182	0.89714	0.81073

C3	C	0.87060	0.91242	0.81087
C4	C	0.91954	0.93518	0.79835
C5	C	0.83459	0.92427	0.79908
C6	C	0.43521	0.68462	0.90345
C7	C	0.44446	0.62631	0.94174
C8	C	0.12539	0.31914	0.85474
C9	C	0.16584	0.36948	0.85177
N10	N	0.09458	0.23365	0.83300
C11	C	0.12816	0.28370	0.83531
N12	N	0.17329	0.41059	0.86765
N13	N	0.93168	0.96278	0.02504
C14	C	0.44849	0.23047	0.89406
C15	C	0.53727	0.24575	0.89420
C16	C	0.58621	0.26851	0.88168
C17	C	0.50126	0.25760	0.88241
C18	C	0.10188	0.01795	0.98678
C19	C	0.11113	0.95964	0.02507
C20	C	0.79206	0.65247	0.93807
C21	C	0.83251	0.70281	0.93510
N22	N	0.76125	0.56698	0.91633
C23	C	0.79483	0.61703	0.91864
N24	N	0.83996	0.74392	0.95098
C25	C	0.57909	0.20393	0.77246
C26	C	0.60185	0.25287	0.78498
C27	C	0.35129	0.76854	0.67988
C28	C	0.29298	0.77779	0.64159
C29	C	0.98581	0.45872	0.72859
C30	C	0.03615	0.49917	0.73156
N31	N	0.90032	0.42791	0.75033
C32	C	0.95037	0.46149	0.74802
N33	N	0.07726	0.50662	0.71568
N34	N	0.62945	0.26501	0.55829
C35	C	0.89714	0.78182	0.68927
C36	C	0.91242	0.87060	0.68913
C37	C	0.93518	0.91954	0.70165
C38	C	0.92427	0.83459	0.70092
C39	C	0.68462	0.43521	0.59655
C40	C	0.62631	0.44446	0.55826
C41	C	0.31914	0.12539	0.64526
C42	C	0.36948	0.16584	0.64823
N43	N	0.23365	0.09458	0.66700
C44	C	0.28370	0.12816	0.66469
N45	N	0.41059	0.17329	0.63235

N46	N	0.96278	0.93168	0.47496
C47	C	0.23047	0.44849	0.60594
C48	C	0.25760	0.50126	0.61759
H49	H	0.85996	0.88429	0.83062
H50	H	0.94881	0.92538	0.80771
H51	H	0.48350	0.63641	0.93218
H52	H	0.09362	0.30977	0.87199
H53	H	0.52662	0.21762	0.91395
H54	H	0.61547	0.25871	0.89105
H55	H	0.15017	0.96974	0.01552
H56	H	0.76029	0.64310	0.95532
H57	H	0.56051	0.19637	0.74893
H58	H	0.59557	0.28347	0.77394
H59	H	0.30456	0.81925	0.64650
H60	H	0.97643	0.42695	0.71135
H61	H	0.88429	0.85996	0.66938
H62	H	0.92538	0.94881	0.69229
H63	H	0.63641	0.48350	0.56782
H64	H	0.30977	0.09362	0.62801
H65	H	0.72679	0.54922	0.93112
H66	H	0.88080	0.39849	0.73237
H67	H	0.06013	0.21589	0.84779
H68	H	0.21589	0.06013	0.65221
Ru69	Ru	0.33333	0.66667	0.91667
Ru70	Ru	0.00000	0.00000	0.00000

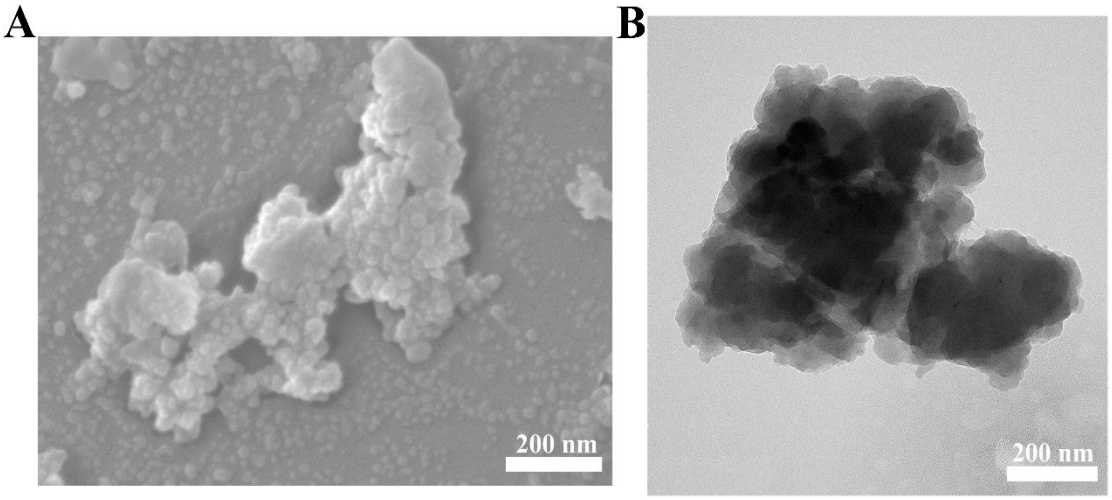

Fig. S3 (A) SEM and (B) TEM images of the Ru-MCOF.

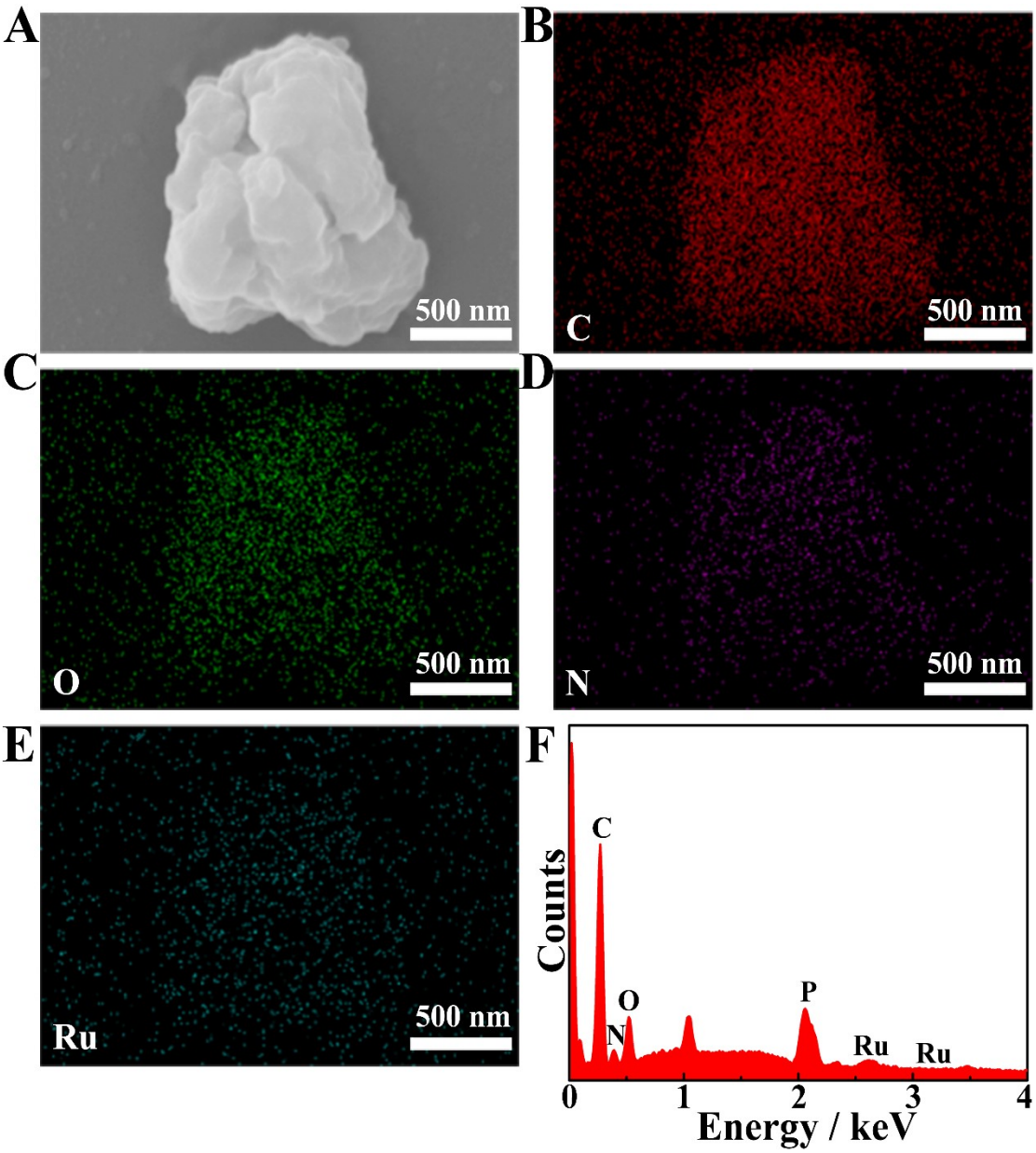

Fig. S4 (A) SEM image and corresponding EDS elemental mapping of the Ru-MCOF for (B) C, (C) O, (D) N, and (E) Ru. (F) EDS spectrum of the Ru-MCOF.

S-2.2 SEM images of the surface of electrodes

As shown in Fig. S5, the surface of Ru-MCOF modified GCE showed irregular morphology, indicating that this ECL biosensor has been successfully constructed.

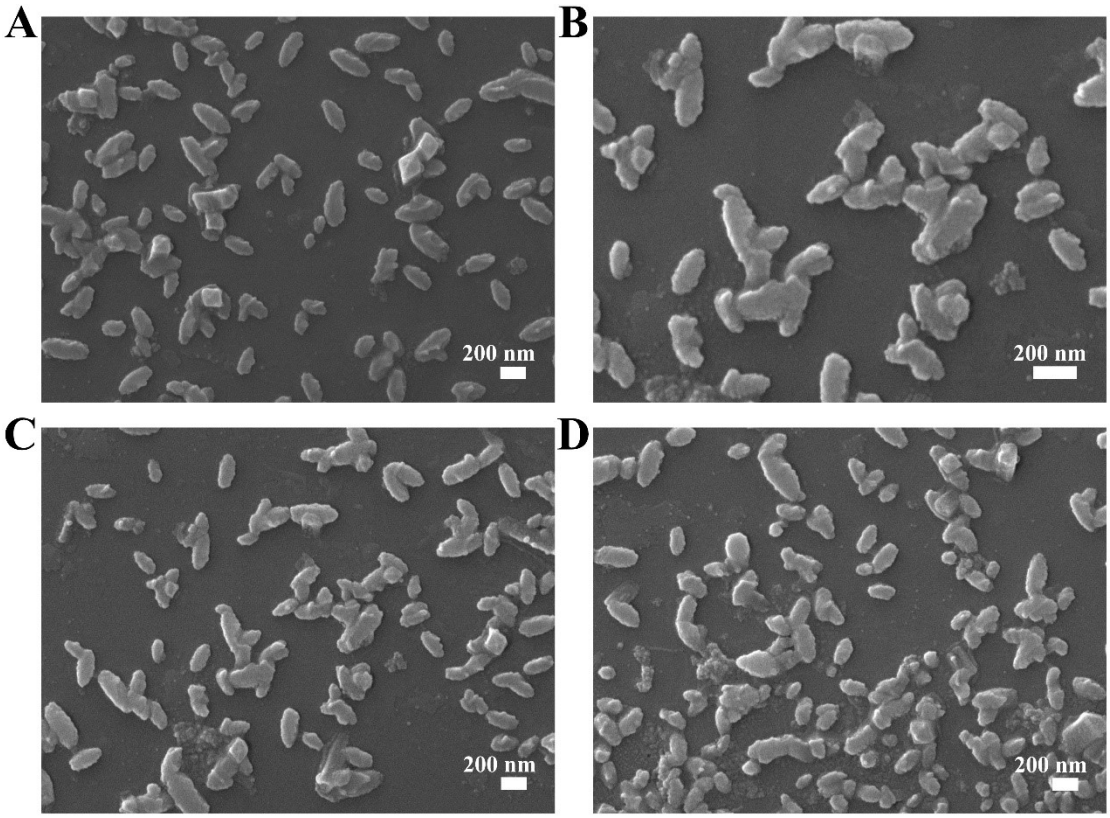

Fig. S5 SEM images of Ru-MCOF modified GCE.

S-2.3 Surface concentration of Ru-MCOF on the electrode surface

In the construction process of the ECL sensor, 10 μL of Ru-MCOF (1 μM) was dropped onto the GCE surface. As displayed in Fig. S5, the SEM images showed that the Ru-MCOF was uniformly distributed on the electrode surface. The surface concentration (c_s) could be evaluated as the following equation:

$$c_s = n_s/S \quad \text{(S1)}$$

where n_s is the mole number of sample added on the electrode surface, and S is the area of the electrode surface.

In this work, the n_s is 10^{-5} μmol and the diameter of the GCE is 4 mm. According to the above equation, the surface concentration of Ru-MCOF on the electrode surface was evaluated as 0.796 μmol/m^2.

S-2.4 ECL efficiency calculation

ECL efficiency was calculated as following equation:[S4]

$$Ø_x = Ø_{st}\left(\frac{\int_0^t Idt}{\int_0^t idt}\right)_x \Big/ \left(\frac{\int_0^t Idt}{\int_0^t idt}\right)_{st} \quad \text{(S2)}$$

$Ø_{st}$ represents the ECL efficiency of $Ru(bpy)_3^{2+}$ (1 mM and 0.1 M $(TBA)BF_4/CH_3CN$, $(TBA)BF_4$ = tetrabutylammonium tetrafluoroborate) *via* annihilation, taken as 5.0%, *I* represents ECL intensity, *i* represents current value and *x* represents the sample.

Table S3 Comparison of ECL efficiencies for different ECL systems

Material	ECL efficiency	Ref.
SnO_2 NC xerogel	0.042%	S5
HHTP-HATP-COF	5.22%	S6
CdS-Ru	8.07%	S7
Ru@MXene	12.50%	S8
Eu(II)-Phen	12.60%	S9
Ru@MOF@NCND-Ru	13.34%	S10
Zn-PTC	15.98%	S11
Zr_{12}-adb	18.22%	S12
CdZnTeS5 QDs	19.78%	S13
Hf-TCBPE	21.72%	S14
Py-sp^2c-CON	25.52%	S15
$[Ru(dcbpy)_3]Cl_2$	2.54%	This work
Ru-MCOF	27.32%	

S-2.5 ECL properties of Ru-MCOF

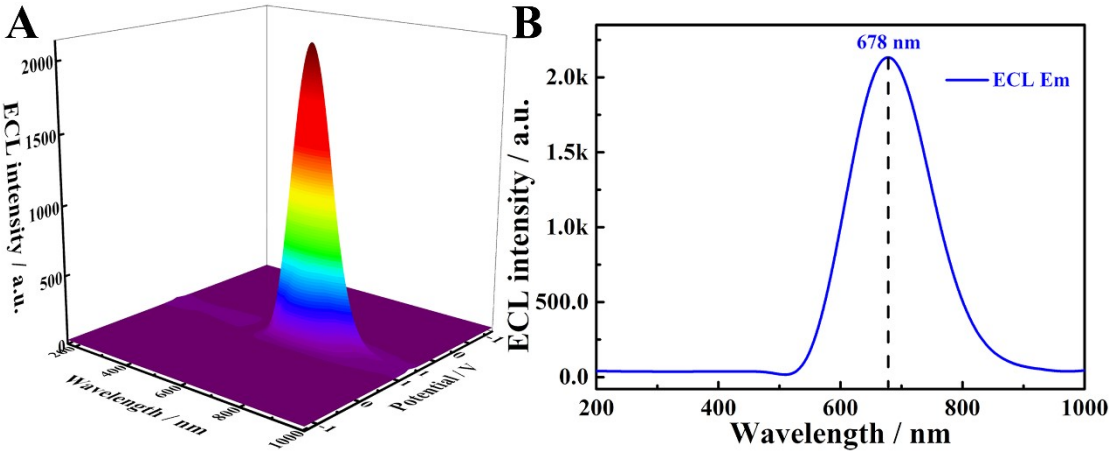

Fig. S6 (A) 3D and (B) 2D ECL spectra of the $[Ru(dcbpy)_3]Cl_2$.

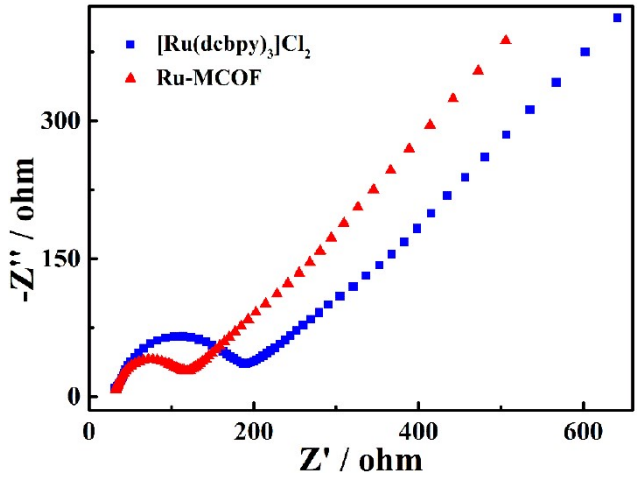

Fig. S7 EIS of the $[Ru(dcbpy)_3]Cl_2$ and Ru-MCOF.

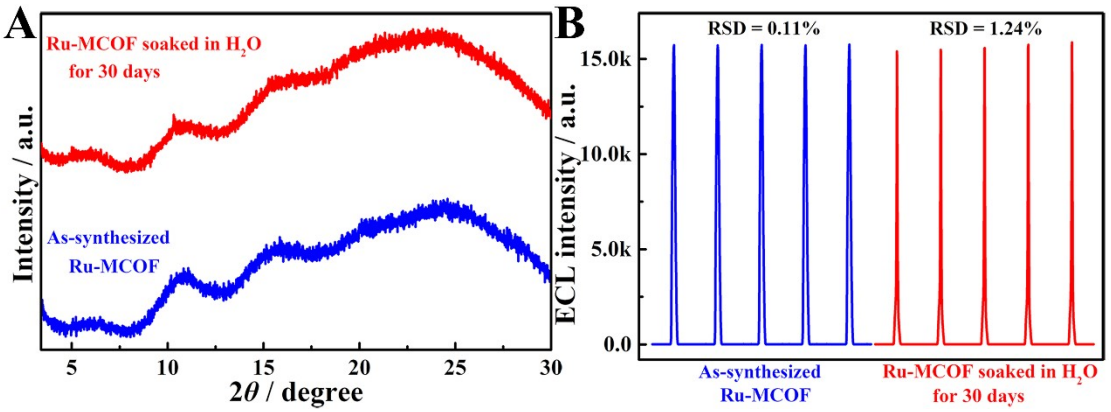

Fig. S8 (A) The PXRD patterns and (B) ECL signals of the Ru-MCOF after soaking in deionized water for 30 days.

S-2.6 ECL mechanism investigation of the Ru-MCOF/TPrA system

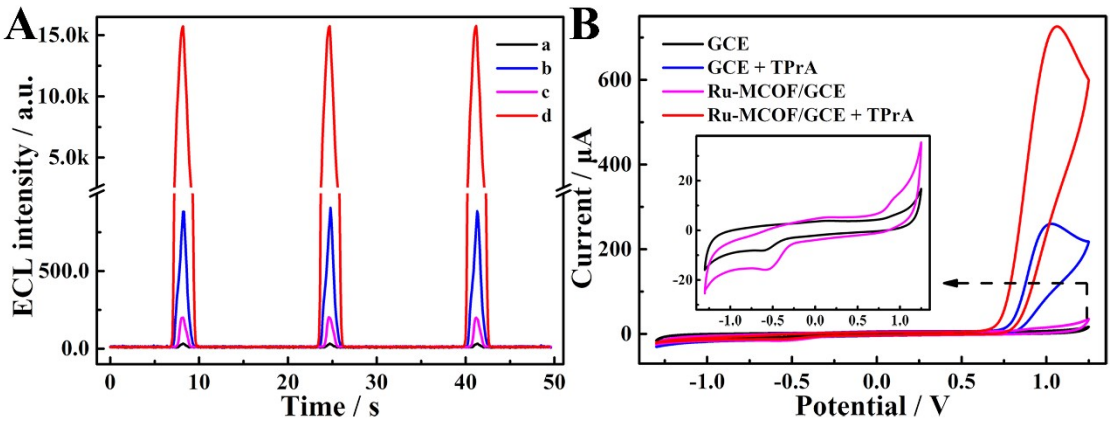

Fig. S9 (A) ECL-time and (B) CV profiles of (a) GCE, (b) GCE + TPrA, (c) Ru-MCOF/GCE, and (d) Ru-MCOF/GCE + TPrA.

S-2.7 Optimization of the experimental conditions

To obtain the best analytical performance of the biosensor, some crucial experimental parameters were optimized. Firstly, the concentrations of the Ru-MCOF were investigated and the corresponding results were displayed in Fig. S10A. It was observed that the ECL response was increased with the concentration of the Ru-MCOF and then decreased after 1 μM. Thus, the optimal concentration of the Ru-MCOF of 1 μM was selected in the following experiments. Then, Fig. S10B plotted the change of the ECL signals with the concentrations of the TPrA. With the concentration increased from 5 to 25 mM, the ECL signal continually increased. When the concentration was more than 25 mM, the ECL signal changed slowly, suggesting that the optimal concentration of the TPrA was 25 mM. Next, according to Fig. S10C, the ECL signal went up with increasing pH from 5 to 7, reaching its maximum at pH 7. The ECL intensity decreased gradually as pH exceeded 7. Therefore, the optimal pH value of the detection environment was obtained at 7.

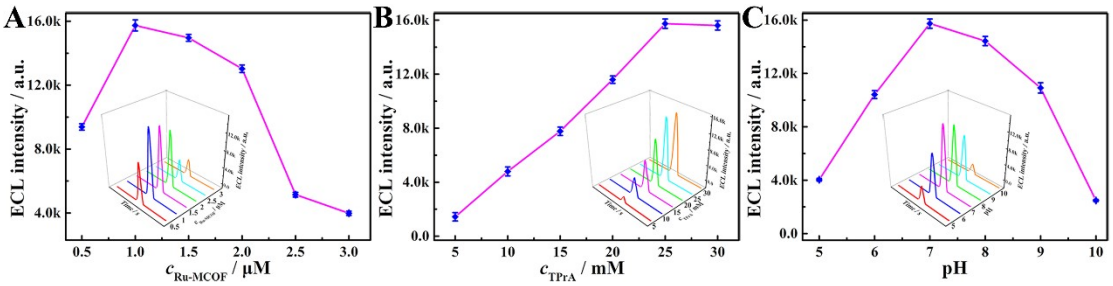

Fig. S10 Effects of (A) concentrations of the Ru-MCOF, (B) concentrations of the TPrA, and (C) pH values of the PBS on ECL intensity. Error bars, SD, n = 3.

The scanning potential range was subsequently studied (Fig. S11). It was obvious that the Ru-MCOF exhibited a strong anodic ECL emission in the scanning potential range of 0 to 1.25 V (Fig. S11A). However, it should be noted that the ECL signal of the Ru-MCOF underwent a gradual decrease because of the instability of the radical cations or the consumption of the TPrA after oxidation. To obtain a relatively stable ECL signal, a negative potential was used to recover those oxidation species back to their precursor molecules *via* an electrochemical reduction procedure.[S16] As shown in Fig. S11B, when the lowest negative potential of -1.3 V was employed, a strong ECL signal with satisfactory stability was obtained. Therefore, -1.3 to 1.25 V was chosen as the optimal scanning potential range in the following experiments. Simultaneously, to prove whether the addition of negative potential altered the excited-state species, CV measurement was performed. As shown in Fig. S11C, the Ru-MCOF exhibited a distinct oxidation peak at 1.06 V (blue line) under the scanning potential range of -1.3 to 1.25 V, which was in accordance with that of the Ru-MCOF in the potential range of 0 to 1.25 V (1.06 V, red line). Furthermore, the Ru-MCOF displayed the maximum ECL emission peak at 669 nm under the scanning potential range of -1.3 to 1.25 V (Fig. 2A and 2B), which was consistent with the ECL emission peak of the Ru-MCOF in the potential range of 0 to 1.25 V (Fig. S11D – S11F). Therefore, we could speculate that

the excited-state species under the scanning potential of -1.3 to 1.25 V were the same as those with the scanning potential range of 0 to 1.25 V.

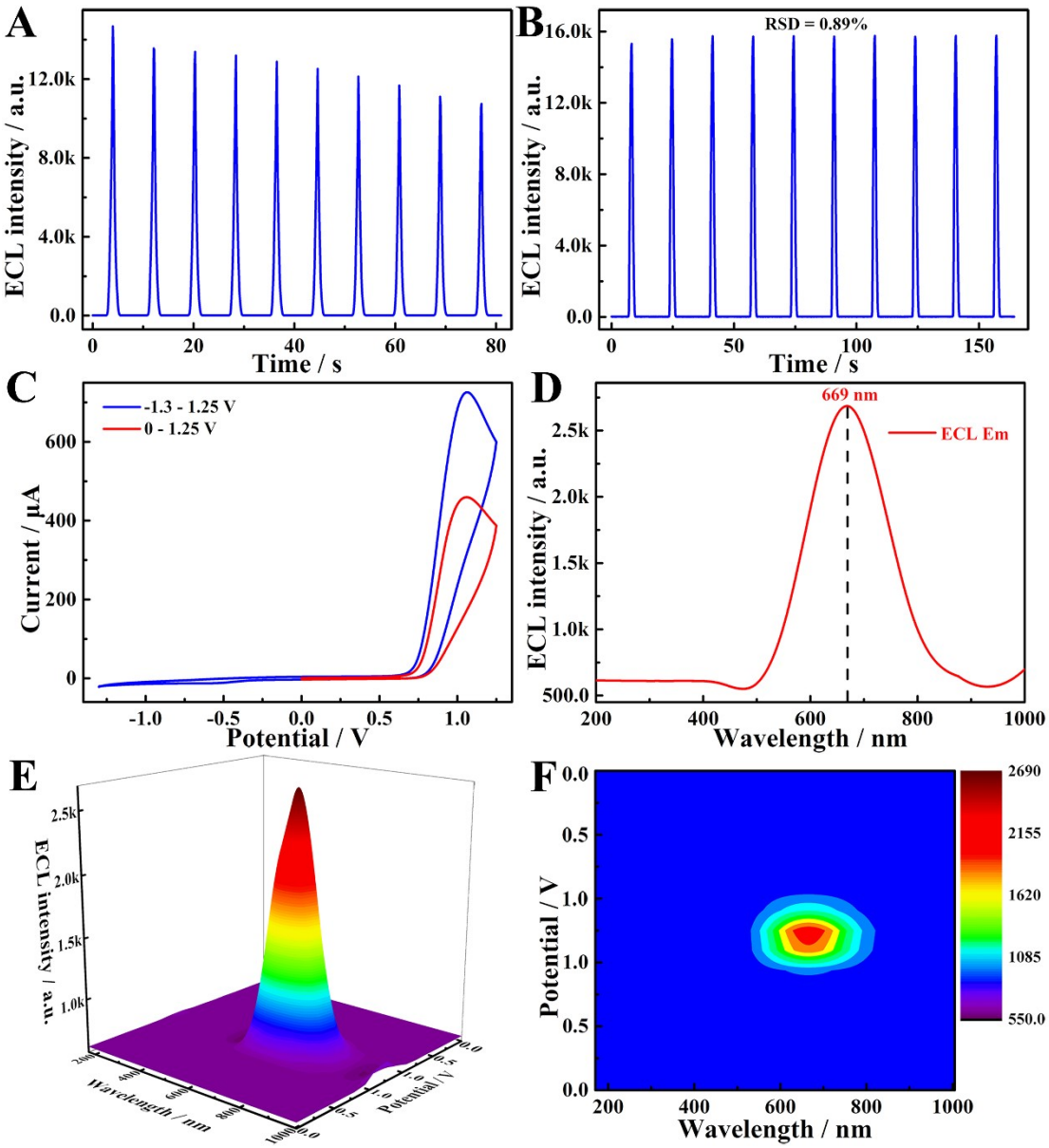

Fig. S11 (A) ECL-time profile of the Ru-MCOF (potential scan of 0 to 1.25 V). (B) ECL-time profile of the Ru-MCOF (potential scan of -1.3 to 1.25 V). (C) CV profiles of the Ru-MCOF (blue line: potential scan of -1.3 to 1.25 V, red line: potential scan of 0 to 1.25 V). (D) 2D and (E) 3D ECL emission spectra of the Ru-MCOF (potential scan of 0 to 1.25 V). (F) Heap map images of the Ru-MCOF (potential scan of 0 to 1.25 V).

Moreover, the preparation time of the DNA rolling machine was optimized. As seen in Fig. S12A, the preparation time from 30 to 110 min led to an increasing ECL signal,

and the maximum platform could be observed at 50 min. Hence, the preparation time of the DNA rolling machine was chosen as 50 min for the most suitable condition in this system. In addition, the rolling time of the DNA rolling machine was also investigated. As illustrated in Fig. S12B, when the rolling time of the DNA rolling machine increased from 20 to 60 min, the ECL signal gradually increased and reached a plateau at 30 min. Therefore, the optimal rolling time of the DNA rolling machine was determined as 30 min at last.

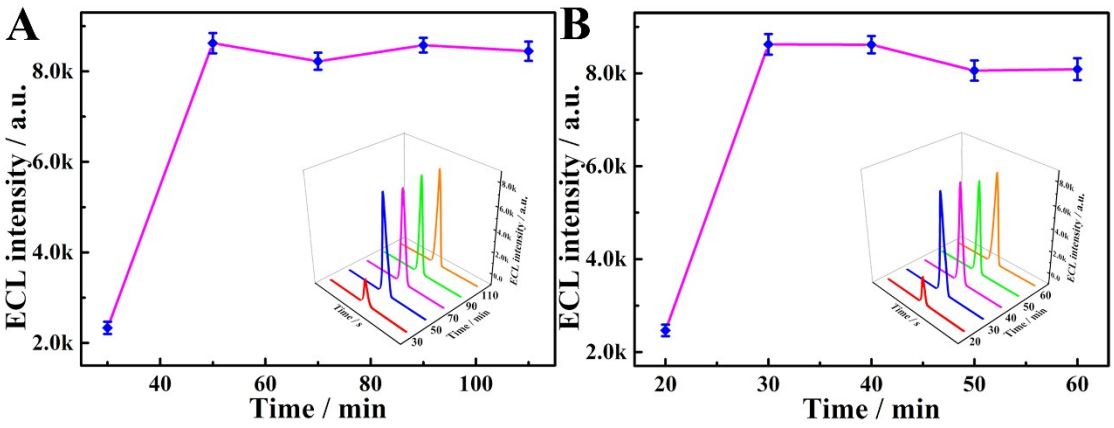

Fig. S12 (A) Optimizing the preparation time of the DNA rolling machine (100 fM miRNA-155). (B) Optimizing the rolling time of the DNA rolling machine (100 fM miRNA-155). Error bars, SD, $n = 3$.

S-2.8 Characterization of the biosensor assembly process

CV and EIS measurements were performed to characterize the stepwise assembly process of the biosensor. As shown in Fig. S13A and S13B, the bare GCE showed a well-defined redox peak and a small resistance (R_{et}) response (curve a), while the Ru-MCOF/GCE showed a decreased peak current and an increased R_{et} response due to the hindrance of the Ru-MCOF on the electron transfer (curve b). When AuNPs were coated on the modified electrode, an obvious increase in peak current and decreased R_{et} response were observed because of the excellent conductivity of AuNPs (curve c). Subsequently, the peak current decreased sequentially while R_{et} response increased

continually for the incubation of H2-Fc (curve d) and HT (curve e), which was attributed to the obstruction of electron transport by nonconductive DNA and HT. Finally, after incubation of the DNA rolling machine and Nb.BbvCI (curve f), the peak current increased and R_{et} response decreased dramatically because of the reduced hindrance of electron transfer.

Moreover, ECL measurement was carried out to further confirm the step-by-step assembly process of the biosensor. As presented in Fig. S13C, almost no ECL signal was observed for the bare GCE (curve a). After the immobilization of the Ru-MCOF, an enhanced ECL signal could be obtained (curve b) owing to the excellent ECL performance of the Ru-MCOF. When AuNPs were dropped on the modified electrode surface, the ECL signal increased once again (curve c) on account of the outstanding conductivity of AuNPs. The ECL signal dramatically decreased after the H2-Fc was successfully incubated on the resultant electrode surface (curve d) due to the quenching effect of Fc. Then, a further decreased ECL signal was obtained with the incubation of HT (curve e) because the electron transfer could be hindered by HT. Ultimately, after the incubation of the DNA rolling machine and Nb.BbvCI (curve f), an increased ECL signal was observed because Fc detached from the electrode surface. All these results indicated the successful assembly of the biosensor.

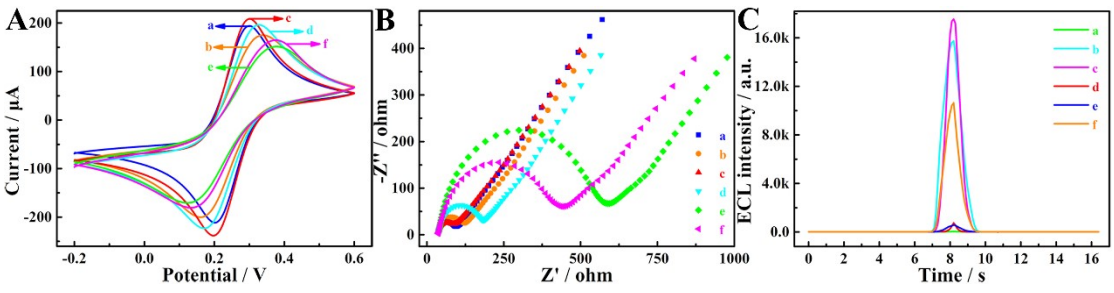

Fig. S13 (A) CV, (B) EIS, and (C) ECL responses of (a) bare GCE, (b) Ru-MCOF/GCE, (c) AuNPs/Ru-MCOF/GCE, (d) H2-Fc/AuNPs/Ru-MCOF/GCE, (e) HT/H2-Fc/AuNPs/Ru-

MCOF/GCE, (f) DNA rolling machine and Nb.BbvCI/HT/H2-Fc/AuNPs/Ru-MCOF/GCE (1 pM miRNA-155).

S-2.9 ECL quenching mechanism by ferrocene (Fc)

As shown in Fig. S13C, when the H2-Fc were assembled on the AuNPs/Ru-MCOF/GCE, a weak ECL response was observed as the "signal off" state (curve d) because of the quenching effect of Fc.[S17-S19] The possible ECL quenching mechanism was depicted as the following equations. First, Fc(II) was oxidized to form Fc(III) at the electrode (eq S3). Then, Fc(III) could react with $TPrA^{\bullet}$ (eq S4), which consumed the $TPrA^{\bullet}$ as the coreactant intermediate of the ECL system to result in the decrease in ECL intensity. Meanwhile, Fc(III) might directly react with Ru^{2+*}-MCOF to reduce the amount of excited state Ru^{2+*}-MCOF through electron transfer (eq S5). Therefore, the ECL emission could be quenched through the above-mentioned pattern.

$$Fc(II) - e^{-} \rightarrow Fc(III) \quad \text{(S3)}$$

$$Fc(III) + TPrA^{\bullet} \rightarrow Fc(II) + Products \quad \text{(S4)}$$

$$Fc(III) + Ru^{2+*}\text{-MCOF} \rightarrow Fc(II) + Ru^{3+}\text{-MCOF} \quad \text{(S5)}$$

S-2.10 Limit of detection (LOD) calculation

LOD was calculated according to a previous report.[S20,S21] Briefly, ECL measurements for the blank sample were carried out with three parallel tests, which exhibited an average ECL intensity (I_B) of 600.59 with a standard deviation (s_B) of 59.22. With a signal-to-noise ratio value (k) of 3, the smallest detectable signal (I_L) could be calculated as

$$I_L = I_B + k \times s_B = 778.25 \quad \text{(S6)}$$

Then the I_L value was put into the linear equation ($I = 32851.37 + 1831.03 \lg c_{miRNA\text{-}155}$) to get the LOD. Finally, the LOD was calculated as 3.02 aM.

S-2.11 Analytical performance of the ECL biosensor

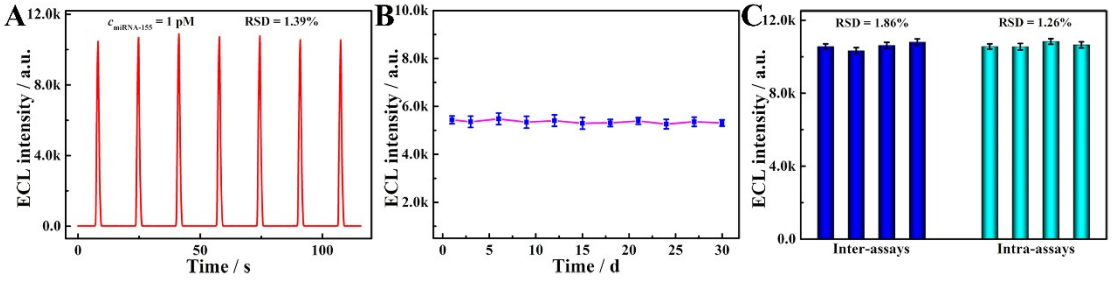

Fig. S14 (A) Stability of the biosensor with 1 pM miRNA-155. (B) Long-term storage stability of the biosensor with 1 fM miRNA-155. (C) Reproducibility of the biosensor with 1 pM miRNA-155. Error bars, SD, n = 3.

Table S4 Comparison of long-term storage stability for different ECL sensors

Number	ECL emitters	Long-term storage stability of sensors	Ref.
1	Ru-MOF-5 NFs	7 days	S22
2	MAPB QDs@SiO_2	7 days	S23
3	$Ru(phen)_3^{2+}$	10 days	S24
4	$Ru(bpy)_3^{2+}$-CS	14 days	S25
5	PEI-lum hydrogel	14 days	S26
6	luminol	14 days	S27
7	PTP/Eu-MOF	15 days	S28
8	EuBTC-Fe_3O_4@Au-Ab_2	20 days	S29
9	PeQDs-NCDs@HZIF-8	21 days	S30
10	Ru-MCOF	30 days	This work

S-3 Notes and references

S1 G. Frens, *Nature Phys. Sci.*, 1973, **241**, 20-22.

S2 L. Pang, J. Li, J. Jiang, G. Shen and R. Yu, *Anal. Biochem.*, 2006, **358**, 99-103.

S3 Z. Dai, J. Zhang, Q. Dong, N. Guo, S. Xu, B. Sun and Y. Bu, *Chin. J. Chem. Eng.*, 2007, **15**, 791-794.

S4 F. Wang, J. Lin, T. Zhao, D. Hu, T. Wu and Y. Liu, *J. Am. Chem. Soc.*, 2016, **138**, 7718-7724.

S5 Y. M. Lei, Y. Zhuo, M. L. Guo, Y. Q. Chai and R. Yuan, *Anal. Chem.*, 2020, **92**, 2839-2846.

S6 J. L. Zhang, L. Y. Yao, Y. Yang, W. B. Liang, R. Yuan and D. R. Xiao, *Anal. Chem.*, 2022, **94**, 3685-3692.

S7 H. Wang, F. Wang, T. Wu and Y. Liu, *Anal. Chem.*, 2021, **93**, 15794-15801.

S8 W. Huang, Y. Wang, W. B. Liang, G. B. Hu, L. Y. Yao, Y. Yang, K. Zhou, R. Yuan and D. R. Xiao, *Anal. Chem.*, 2021, **93**, 1834-1841.

S9 L. Zhao, X. Song, H. Wang, X. Wang, D. Wu, Q. Wei and H. Ju, *Chem. Eng. J.*, 2022, **446**, 136912.

S10 D. Bahari, B. Babamiri, K. Moradi, A. Salimi and R. Hallaj, *Biosens. Bioelectron.*, 2022, **195**, 113657.

S11 J. M. Wang, L. Y. Yao, W. Huang, Y. Yang, W. B. Liang, R. Yuan and D. R. Xiao, *ACS Appl. Mater. Interfaces*, 2021, **13**, 44079-44085.

S12 L. Y. Yao, F. Yang, G. B. Hu, Y. Yang, W. Huang, W. B. Liang, R. Yuan and D. R. Xiao, *Biosens. Bioelectron.*, 2020, **155**, 112099.

S13 X. L. Liang, N. Bao, X. Luo and S. N. Ding, *Biosens. Bioelectron.*, 2018, **117**, 145-152.

S14 W. Huang, G. B. Hu, L. Y. Yao, Y. Yang, W. B. Liang, R. Yuan and D. R. Xiao, *Anal. Chem.*, 2020, **92**, 3380-3387.

S15 J. L. Zhang, Y. Yang, W. B. Liang, L. Y. Yao, R. Yuan and D. R. Xiao, *Anal. Chem.*, 2021, **93**, 3258-3265.

S16 D. Xiao, Y. Xian, L. Liu, Z. Gu and B. Wen, *New J. Chem.*, 2014, **38**, 902-905.

S17 W. Cao, J. P. Ferrance, J. Demas and J. P. Landers, *J. Am. Chem. Soc.*, 2006, **128**, 7572-7578.

S18 J. L. Liu, J. Jiang, J. Q. Zhang, Y. Q. Chai, Q. Xiao and R. Yuan, *Biosens. Bioelectron.*, 2020, **152**, 112006.

S19 J. L. Liu, Y. Zhuo, Y. Q. Chai and R. Yuan, *Chem. Commun.*, 2019, **55**, 9959-9962.

S20 G. L. Long and J. D. Winefordner, *Anal. Chem.*, 1983, **55**, 712-724.

S21 A. Chen, M. Zhao, Y. Zhuo, Y. Chai and R. Yuan, *Anal. Chem.*, 2017, **89**, 9232-9238.

S22 X. Dong, Y. Du, G. Zhao, W. Cao, D. Fan, X. Kuang, Q. Wei and H. Ju, *Biosens. Bioelectron.*, 2021, **192**, 113505.

S23 J. Li, Q. Wang, C. Xiong, Q. Deng, X. Zhang, S. Wang and M. M. Chen, *Food Chem.*, 2022, **390**, 133200.

S24 L. Yang, Y. Zhang, R. Li, C. Lin, L. Guo, B. Qiu, Z. Lin and G. Chen, *Biosens. Bioelectron.*, 2015, **70**, 268-274.

S25 J. Huang, Y. Xiang, J. Li, Q. Kong, H. Zhai, R. Xu, F. Yang, X. Sun and Y. Guo, *Biosens. Bioelectron.*, 2021, **194**, 113601.

S26 Y. Duan, Y. Song, N. Fan, Y. Yao, S. Deng, S. Ding, B. Shen and Q. Yin, *Biosens. Bioelectron.*, 2022, **197**, 113784.

S27 Z. Sun, J. Lu, X. Zhang, X. Shan, Q. Wu, Y. Zhao and L. Tian, *Microchim. Acta*, 2022, **189**, 99.

S28 J. Li, M. Luo, C. Jin, P. Zhang, H. Yang, R. Cai and W. Tan, *ACS Appl. Mater. Interfaces*, 2022, **14**, 383-389.

S29 L. Zhao, X. Song, X. Ren, H. Wang, D. Fan, D. Wu and Q. Wei, *Biosens. Bioelectron.*, 2021, **191**, 113409.

S30 Y. Cao, Y. Zhou, Y. Lin and J. J. Zhu, *Anal. Chem.*, 2021, **93**, 1818-1825.